Experimental and theoretical study of filtered optical feedback in a semiconductor laser

Experimental and Theoretical Study of Filtered Optical Feedback in a Semiconductor Laser

Alexis P. A. Fischer, Ole K. Andersen, Mirvais Yousefi, Steven Stolte, and Daan Lenstra

***Abstract*—We report on the systematical investigation of the steady-state regime and the dynamical behavior of a semiconductor laser subject to delayed filtered optical feedback. We study a Fabry–Perot (FP) interferometer type of filter placed in the external feedback loop of a diode laser. The effects of the filter on the locking of the diode laser frequency to the external cavity modes are described. We report and observe hysteresis, bistability, and multistability and show that all these are well described by a set of rate equations for the coupled laser and FP cavity system. We also present an experimental stability diagram that summarizes the dynamical behavior of the system.**

***Index Terms*—Diode laser, external cavity modes, Fabry–Perot type filter, filtered feedback, hysteresis, locking, multistability, stability diagram.**

I. Introduction

DIODE lasers are known to be extremely sensitive to any external perturbation. Different kinds of optical perturbations exist, such as optical injection [1] or optical feedback from a conventional mirror [2] or from a phase-conjugate mirror [3]. They have all been intensively studied both theoretically and experimentally in order to understand why the performance of a diode laser (DL) is sometimes improved and sometimes degraded by these perturbations.

Theoretically, the problem has been approached by using a set of rate equations [4]. From this, it appeared that the stability of a DL is mainly governed by two parameters: the amount of feedback and, in the case of a coherent perturbation, the phase difference between the emitted wave and the perturbation wave.

Of the above-mentioned perturbation schemes, conventional optical feedback (COF) has proven to be a very interesting way of controlling the stability of a DL. For instance, it has been shown that the operation frequency of a DL can be locked to one of the external-cavity modes allowing for a linewidth reduction [5]. However, direct applications would require a precise mechanical and thermal control of the external cavity in order to achieve longterm stability, which is difficult. In fact, a parasitic change in the external-cavity length of the order of a wavelength could already cause the frequency to jump from one external cavity mode to another. Apart from this parasitic mode hopping, the control of the amount of feedback is also important because of the possible undamping of the relaxation oscillations [6]. Multistability, i.e., the fact that for a given feedback strength the DL has several stable operation modes to choose from, has been reported in [7]. Potential applications of COF are in the area of optical telecommunications where feedback is already used in order to obtain light sources that are stable and have a narrow linewidth with strongly suppressed jitter and frequency drifts. However, the mechanical problems concerning the stability of the external cavity are identical to what has been said above.

Other structures have been reported in which a medium is placed within the external cavity. This medium could be an alkali metal vapor. Locking of the DL frequency to transition lines of rubidium [8] and barium [9] has been demonstrated. Other groups have locked the frequency of a DL to the resonance of a Fabry–Perot (FP) interferometer placed within the external cavity [10]. All these systems are equivalent to a DL with an external cavity containing a frequency-selective filter. Surprisingly, in all these works, the dynamical aspects of such a system are not adressed, and little is said about the relaxation oscillations.

We present here a systematic experimental and theoretical investigation of the steady-state regime and the dynamical behavior in order to understand the locking mechanism of such a system. In Section II, the experimental setup is described. Sections III and IV report, respectively, on the experimental results and the stability diagram. In Sections V and VI, a theoretical model for the system is presented and simulated. In Section VII, the simulations are compared with experiment.

The main goal of this paper is to provide a complete physical picture of the filtered optical feedback properties, in order to explain the interaction between diode lasers and filters placed in the external feedback loop.

II. Experimental Setup

The experimental setup is shown in Fig. 1. It consists of a DL with an external-cavity loop, including a filter, and a diagnostic branch. The DL used is a commercial single-mode 5-mW FP-type semiconductor laser (SHARP LT027) emitting at 780 nm, and having a threshold current of 42 mA (free-running). The external-feedback loop consists of the following elements: a linear polarizer (P), a 50:50 beamsplitter (BS1), an optical isolator (I1), another 50:50 beamsplitter (BS2), a frequency-selective optical filter (FP filter) consisting of a two-plane-mirror FP interferometer, and a second optical isolator

Manuscript received August 11, 1999; revised December 6, 1999. This work was supported in part by the EU-project FALCON, ERB 4061 PL97-0131 and by the 'Stichting voor Fundamenteel Onderzoek der Materie' (FOM) which is financially supported by the 'Nederlandse Organizatie voor Wetenschappelijk Onderzoek' (NWO).

A. P. A. Fischer is with the Laboratoire de Physique des Lasers, Universite Paris 13 Villetaneuse, 93430 Villetaneuse, France.

O. K. Andersen, M. Yousefi, S. Stolte, and D. Lenstra are with the Faculty of Sciences, Vrije Universiteit, De Boelelaan 1083, 1081 HV Amsterdam, The Netherlands.

Publisher Item Identifier S 0018-9197(00)01844-3.

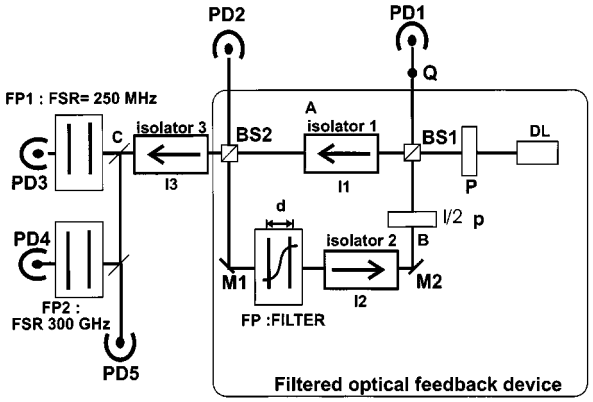

Fig. 1. The experimental setup. DL: diode laser; BS: beamsplitter; I: optical isolator; PD: photodetector; FPI: FP interferometer; FP: filter; and P: polarizer.

(I2), followed by a half-wave plate (λ/2P). A calibrated powermeter can be placed at point Q to measure the absolute power of the feedback light.

The path of the light is as follows. Light emitted by the DL passes through P whose direction of polarization is the same as the polarization of the light from the DL. The polarizer is misaligned slightly to avoid parasitic feedback into the DL. The light is split by BS1 into two branches denoted A and B. BS1 is also tilted so as to avoid parasitic reflections from its facets. The light in branch B is blocked by isolator I2 (–43 dB) whereas the light in arm A is transmitted through isolator I1 (–41 dB) to BS2. The polarization at the output of I1 is tilted 45 degrees with respect to the polarization of P. BS2 splits the power into two parts; one goes into the diagnostic branch C, which is isolated from the feedback loop by isolator I3 (–39 dB). The other part of the light is sent to the filter via the mirror M1. The filter consists of two plane-parallel mirrors separated by the distance d and is characterized by multiple resonances with a free spectral range (FSR) of $c/2d$, where c is the speed of light. The finesse was estimated to approximately $f = 8$. The light reflected by the filter is split by BS2. Half of the power is blocked by I1, and the other half is sent to a slow 100–kHz bandwidth photodetector (PD2). The light transmitted through the filter is passed through I2. At this point, the polarization of the light is rotated 90 degrees with respect to the direction of P. To compensate for this, the light is passed through a $\lambda/2$ plate that allows for the direction of polarization to be rotated. In order to control the alignment of the feedback, the mirror M2 is mounted on a translation stage. The light is then split by BS1, half of which is sent to a slow 100-kHz bandwidth photodetector (PD1), and the other half is sent through P and fed back into the DL. The total length of the external cavity is $L = 1.80$ m, resulting in a separation of 170 MHz between the external cavity modes. The amount of feedback is controlled through the combination of the $\lambda/2$ plate and the polarizer P. When the light is polarized perpendicularly with respect to P, there is no feedback and the DL is free-running. The losses along the loop, the $\lambda/2$ plate and the polarizer, result in a maximum isolation level of –60 dB. Using the $\lambda/2$ plate to turn the polarization away from the perpendicular position increases the transmission through P. The maximum amount of power measured in point Q with a power meter and at one of the peaks of the filter was 30 μW, corresponding to a feedback level up to –22 dB. This has been measured for a polarization of the light at the output of the $\lambda/2$ plate perpendicular to the direction of P.

The diagnostic branch consists of a 250-MHz FSR FP interferometer with a finesse $F = 30$ that can be operated in either a scanning mode or stationary mode, a 300-GHz FSR wavemeter (Burleigh), a photodiode PD5 for detecting the power of the DL, and a 300-GHz FSR FP etalon with a finesse $f = 2$. The 300-GHz FSR FP etalon is used for measuring the relative frequency. The combination of a large FSR and a low finesse makes it possible to have the DL frequency operating on one of the slopes of the interferometer resonances. This, in turn, establishes a relation between the transmitted power through the FP etalon and the frequency of the DL that is linear to a good approximation. In this way, frequency changes (due to feedback) are transformed into power changes, and the relative frequency can be determined as the ratio between the powers measured at PD4 and PD5.

Four different filters with mirror spacings of, respectively, $d = 25$ mm, $d = 12.4$ mm, $d = 5.4$ mm, and $d = 2.4$ mm have been used. The corresponding FSR's are 6.4 GHz, 12.4 GHz, 28 GHz, and 63 GHz. The full-width at half-maximum (FWHM) of the filters are 800 MHz, 1.55 GHz, 3.5 GHz, and 7.9 GHz, respectively.

III. Results

The frequency-dependent response of the filter with a 6.4-GHz FSR is shown in Fig. 2(a). It has been obtained by scanning the pump current of the DL between 50 and 65 mA with a triangular waveform. The frequency of the DL follows the current linearly without any jump to other longitudinal modes. The feedback was minimized by tuning the $\lambda/2$ plate. A residual feedback level of approximately –55 dB was measured, but, according to [6] and in accordance with our observations, such a low feedback has no observable effect on the laser's behavior. The frequency-dependent response of the filter is then monitored using PD1. The upper trace is the current versus time, while the lower trace is the transmitted power through the filter versus time. Both traces are synchronized. The response of the filter shows two resonances for both the increasing and decreasing ramp of the current.

Fig. 2(b) shows the same curves in the case where the feedback level at the center of the resonance was 0.5 μW (–40 dB). The response curve of the filter exhibits a discontinuous trace, very similar to the one measured without feedback except that it looks "digitized." We distinguish four "points" which correspond to the four 170-MHz-separated, external-cavity modes within the 800-MHz filter width. With the other filters available, it was verified that the number of external-cavity modes indeed changes proportionally to the filter width.

Increasing the amount of feedback to ~4 μW (–31 dB) causes some asymmetries to appear in the response curve of the filter. First, the resonance amplitude appears smaller for increasing current than for decreasing current. Another asymmetry occurs within the peaks. For an amount of feedback corresponding to 6 μW (–29 dB), a frequency jump is observed. This can be seen in Fig. 2(c) as the missing right flank in each resonance. With increasing feedback, this effect is first observed for decreasing

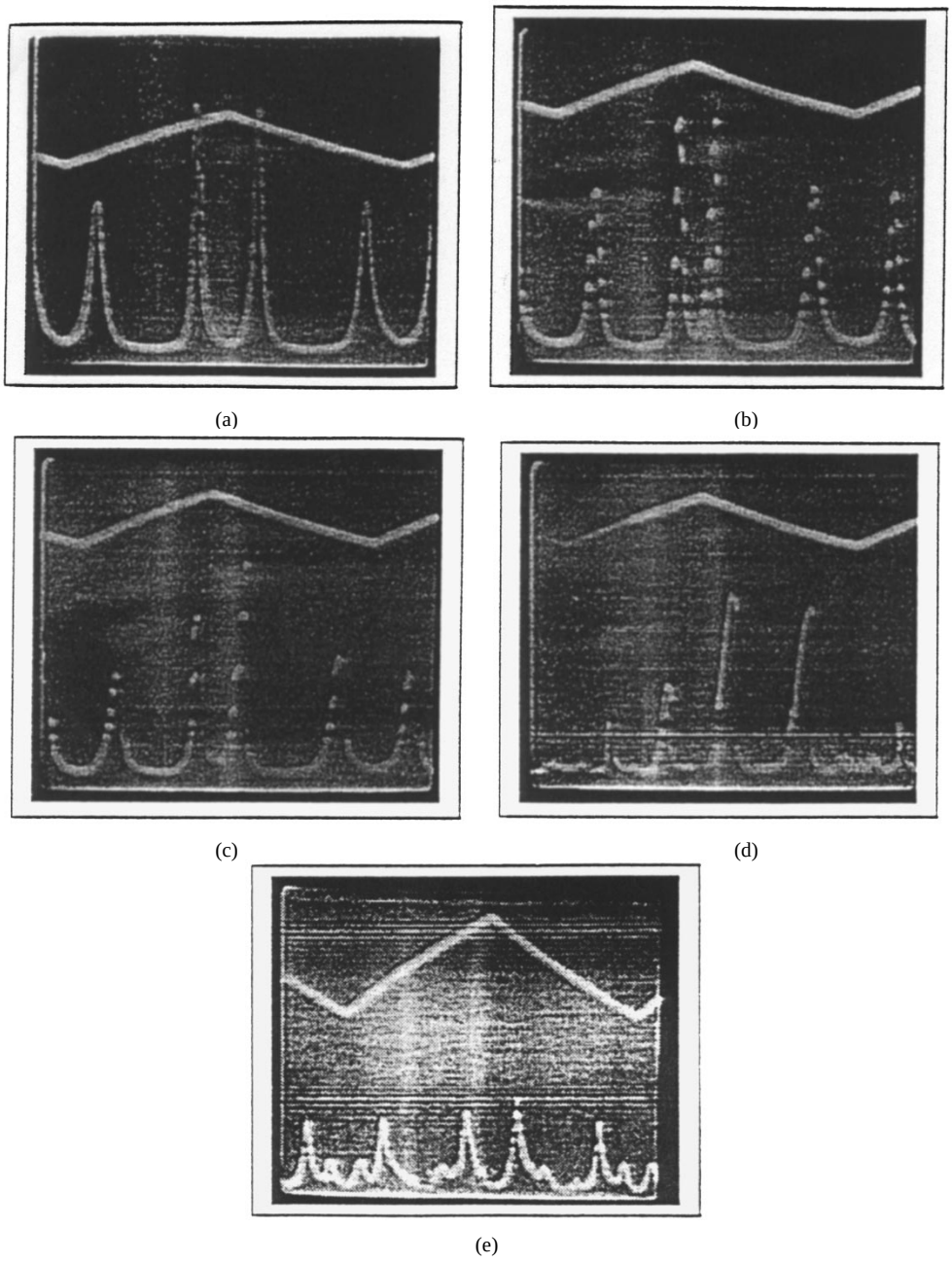

Fig. 2. Experimentally obtained filter profiles obtained by scanning the pump current of the DL, upper trace of each figure, up and down. Five cases for different levels of feedback are shown. (a) No feedback (−55 dB). (b) Low feedback (−40 dB). (c) Moderate feedback (−31 dB). (d) High feedback (−29 dB). (e) Undamping of the relaxation (−26 dB) oscillation.

current. The frequency jumps approximately 700 MHz from a position corresponding to the top of the peak to its foot. This phenomenon occurs for both increasing and decreasing current and hence is not dependent on the sign of dP_f/dJ, where P_f is the power transmitted through the filter. The jump only occurs for negative slope versus time, i.e., $dP_f/dt < 0$. The effect therefore depends on the history of the system, and it suggests hysteresis.

Fig. 2(d) shows the case for a feedback level of 9 μW (−28 dB). A continuous trace is observed, indicating that the laser locks to one of the external cavity modes. This phenomenon occuring on the left flank is followed by a jump from the top of the peak to its foot.

Increasing the feedback to 14 μW (−26 dB) causes the relaxation oscillation to undamp, as seen by the small sidebands in Fig. 2(e). The relaxation oscillation sidebands are located 3.2 GHz from the center of the filter resonance. Also, the frequency jump on the right side of the flanks is not observed. Further increasing the feedback results in longitudinal mode jumps.

As shown in Fig. 3, the frequency of the DL locks to the left (right) flank of the filter resonance when increasing (decreasing) the current. This is a source of proof of hysteresis in the system. These results were derived for the case of a feedback level of 9 μW (−28 dB). For comparison, the filter profiles are shown in the lower figure. Hysteresis is observed close to

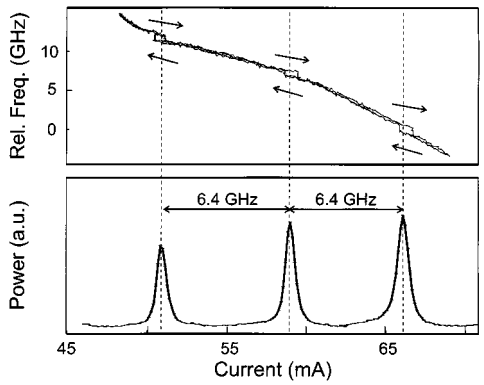

Fig. 3. Experimentally observed multistability. The frequency of the DL locks to the multiple resonances of the FP filter. Arrows indicate the direction of time. Upper part: hysteresis loop in frequency versus pump current. Lower part: power transmission through the filter versus pump current.

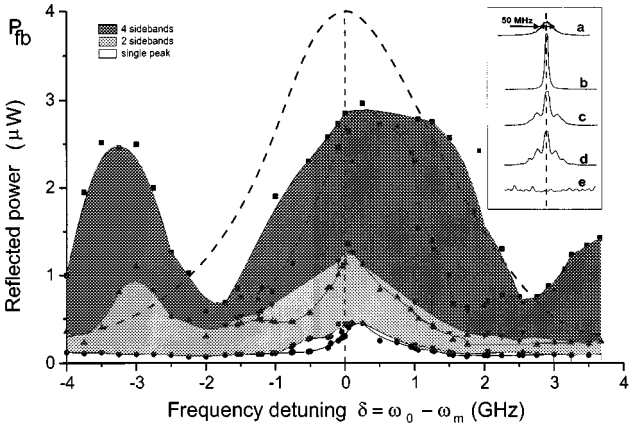

Fig. 4. Stability diagram. The inset shows the different dynamical behaviors. (a) Free running. (b) Linewidth reduction. (c) Undamping of relaxation oscillation. (d) Undamping with four sidebands. (e) Broad spectrum. Opaque circle: boundary of the free-running behavior; opaque triangles: boundary of the linewidth reduction region; opaque square: boundary of the RO undamping region. The dashed line indicates the filter profile.

all three resonances. In this case, the amplitude of the current scan was increased compared to Fig. 2(d) so as to include three resonances.

These measurements are clear evidence of multistability [2]. Decreasing the FSR of the filter will increase the number of resonances inside the same DL tuning range and will produce an increased number of hysteresis loops and multistabilities.

IV. Dynamical Behavior: Stability Diagram

The relaxation oscillations (RO's) appear to undamp progressively when the maximum amount of power, measured at the filter resonance frequency, is increased. As can be seen in Fig. 2(e), the RO's are even undamped when the DL frequency is different from the resonance frequency of the filter. We have investigated systematically the conditions under which the RO's are undamped. The experimental results are collected in the stability diagram in Fig. 4. This diagram shows the behavior of the DL in the plane spanned by the detuning $\delta = \omega_0 - \omega_{\rm m}$ between the free-running DL frequency ω_0 and one of the resonance frequencies of the filter $\omega_{\rm m}$ (horizontal), and the feedback power P_{fb} (vertical).

To investigate the stability of the DL systematically, we proceed as follows. The pump current is fixed so that the detuning δ is kept constant while P_{fb} is changed by adjusting the $\lambda/2$ plate. The behavior of the DL is then diagnosed by the optical spectra obtained by the interferometer and checked with the wavemeter. The amount of feedback at which the spectrum of the DL abruptly changes is then recorded. In this way, the stability diagram is decomposed into zones of different dynamical behavior. Thus, the diagram in Fig. 4 has been obtained for the filter with mirror spacing $d = 5.4$ mm (28-GHz FSR, 3.5-GHz FWHM).

For small values of P_{fb}, the DL is observed to operate single mode but with a linewidth that is narrowed compared to its free-running value. This is indicated by the white region in Fig. 4. The free-running spectrum is shown in (a) of the inset; an example of the linewidth narrowing recorded in the white area is shown in (b) of the inset. The shape of this region resembles the filter profile with a maximum at the filter resonance. Note that, even for large detunings, linewidth narrowing is observed.

Above the linewidth narrowing range, two zones are found corresponding to the behaviors (c) and (d) of the inset of Fig. 4. These zones are indicated with, respectively, light gray and dark gray. The light gray zone corresponds to the undamping of the RO with two side bands 3.2 GHz away from the central peak. The dark gray zone corresponds to the undamping of the RO with four sidebands symetrically located around the central peak at 3.2 and 6.4 GHz. Note that all these zones are larger than the filter width and are more pronounced for positive detunings. This is due to the α-parameter that leads to a red shift of the laser frequency as a result of feeding light back into the laser cavity. Consider the case of positive detuning, i.e. the frequency of the DL is to the blue with respect to the filter. The effect of the filtered feedback is to lock the DL frequency to the flank of the filter resonance. The effect of the α-parameter is to shift the DL frequency to the red when feeding light back into the laser cavity. Hence, in the case of positive detunings (right flank of the filter), both mechanisms tend to shift the DL frequency in the same direction. For negative detunings, the frequency shift due to the α-parameter and the shift due to the filtered optical feedback are in opposite directions. Therefore, the locking region extends further into positive detunings than negative detunings. This explains the asymmetry observed.

It should be noted that, for some detunings, the bounds of the zones appear to differ. This is a consequence of the hysteresis mentioned above.

Note that increasing the feedback level further does not result in coherence collapse. However, this behavior, shown in (e) of Fig. 4, was observed using the filter with larger bandwidth, i.e., for $d = 2.4$ mm. For the filter with $d = 12.4$ mm, only behaviors (a)–(c) were observed. The reason is that power in the sidebands outside the bandwidth of the filter is not fed back into the laser and, thus, effectively saturates the feedback level. This phenomenon is similar to what was observed in [11].

V. Theory

For the theoretical analysis of the laser dynamics in the case of filtered external optical feedback, we will assume a

Lorentzian filter L characterized by a FWHM 2Λ, and by the central frequency ω_m, i.e.,

$$L(x) = \frac{\Lambda}{\Lambda + i(x - \omega_m)} \tag{1}$$

Since in the experiment the laser was always observed to operate in a single longitudinal mode, a single-mode model will be used. In a slowly varying envelope approach, such that the full electrical field is given by $\mathrm{Re}\{E(t)e^{i\omega_0 t}\}$, where ω_0 is the solitary laser frequency and τ is the external cavity round-trip time, the laser dynamics in the case of external feedback with a Lorentzian filter can be described by the set of rate equations [12]

$$\begin{aligned}
\dot{E}(t) &= \frac{1}{2}(1 + i\alpha)\xi n(t)E(t) + \gamma F(t) \\
\dot{n}(t) &= -\beta n(t) - (\Gamma_0 + \xi n(t))(P(t) - P_0) \\
\dot{F}(t) &= i[\Lambda E(t - \tau)e^{-i\omega_0 \tau} + (\omega_m + i\Lambda)F(t)].
\end{aligned} \tag{2}$$

Here, n is the inversion normalized to its threshold value, F is the field fed back into the laser cavity, $P = |E|^2$ is the photon number, $\beta = (1 + T_1\xi P_0)/T_1$ where $P_0 = (J - J_{\mathrm{thr}})/\Gamma_0$ is the photon number under solitary laser operation conditions, α is the linewidth enhancement factor, ξ is the differential gain coefficient, γ is the feedback rate, T_1 is the carrier lifetime, Γ_0 is the photon decay rate, and J and J_{thr} are the pump current and its threshold value. Noise is not included in the analysis.

It is a well-known fact that the solitary laser frequency changes with the pump current [4]. We will therefore take the solitary laser frequency ω_0 as

$$\omega_0 = \omega_0(J) = \omega_{\mathrm{thr}} - k(J - J_{\mathrm{thr}}) \tag{3}$$

where ω_{thr} is the solitary laser frequency at the onset of lasing and $k > 0$ is a proportionality constant whose value will be derived from experiment. Note that, due to the positive sign of the linewidth enhancement factor α, the frequency shifts to the red as the pump strength is increased.

The first step is to investigate the steady-state regime of the filtered external optical feedback system by means of a fixed point analysis of (2). In other words, we are looking for situations where the DL exhibits monochromatic operation with time-independent frequency detuning $\Delta\omega = \omega - \omega_0$ from the solitary laser frequency $\omega_0(J)$ and time-independent amplitude E_S. Hence, ω is the new frequency of the DL with filtered external optical feedback. We therefore assume the following form for the fixed point solutions:

$$\begin{aligned}
E(t) &= E_S e^{i\Delta\omega t} \\
F(t) &= F_S e^{i(\Delta\omega t + \phi)} \\
n(t) &= n_S
\end{aligned} \tag{4}$$

Here E_S, F_S, n_S, $\Delta\omega$ and ϕ are real, time-independent quantities. By insertion of (4) into (2) a transcendental equation in $\Delta\omega$ can be derived, reading

$$\begin{aligned}
\Delta\omega\tau = -f(\Delta\omega)C\sin[&(\Delta\omega + \omega_0(J))\tau \\
&+ \arctan(\alpha) - \arctan(\Lambda/(\Delta\omega - \omega_m))]
\end{aligned} \tag{5}$$

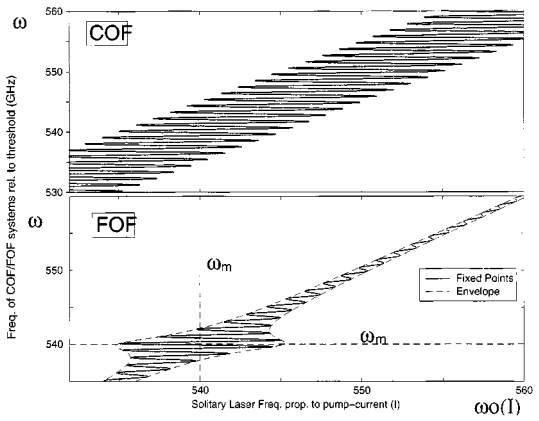

Fig. 5. The frequency ω of the DL plotted versus the solitary laser frequency ω_0 in the cases of (a) COF and (b) filtered external optical frequency. The solid line is the external-cavity mode structure and the dashed curve indicates the envelope of the filter profile. ω_m is the central frequency of the filter.

where the function f is the absolute value of (1),

$$f(x) = \frac{\Lambda}{\sqrt{\Lambda^2 + (x - \omega_m)^2}} \tag{6}$$

and $C \equiv \tau\gamma\sqrt{1 + \alpha^2}$ is the dressed feedback strength. Equation (5) is solved numerically for $\Delta\omega$. Each solution defines a fixed point solution of (2), corresponding to a mode or antimode of the compound system.

From (5), it is realized that, for no feedback, i.e., $\gamma = 0$, the only solution is $\Delta\omega = 0$, meaning that the laser operates as a solitary laser. Furthermore, it is instructive to rederive the well-known version of (5) in the case of COF. Thus, in the limit of a wide filter, (5) transforms into

$$\Delta\omega\tau = C\cos[(\Delta\omega + \omega_0(J))\tau + \arctan(\alpha)]. \tag{7}$$

This is the equation for the fixed points of a semiconductor laser with conventional optical feedback. This result differs from the usual in that the cosine replaces the sine. This is a trivial consequence of the i convention in (1) and does not affect the real physics in that way. The number of fixed points given by (7) is roughly given by $2C/\pi$. Increasing C results in a pairwise creation of fixed points as a result of subsequent saddle-node bifurcations [13], which exactly corresponds to the birth of a mode and an antimode of the compound system simultaneously.

In order to explain the role of the filter, let us compare the situation of filtered external optical feedback with COF. The frequency $\omega = \omega_0 + \Delta\omega$ of the DL with filtered external optical feedback will be investigated as a function of the solitary laser frequency. There are two reasons for doing this: 1) the solitary laser frequency ω_0 is controlled by the pump current applied to the DL and thus is a parameter directly accessible experimentally and 2) the main effect of feeding light back into the DL is to induce a frequency shift $\Delta\omega$ with respect to ω_0. Therefore, ω as a function of ω_0 is a very useful characterization of the system.

In Fig. 5, ω is plotted as a function of ω_0 as determined by (5) for the cases of COF [see Fig. 5(a)] and filtered external optical frequency [see Fig. 5(b)].

In the case of COF, the fixed points lie on a "snake"-like contour. This is a consequence of the sine function in (7) that corresponds to the compound cavity modes. The modes are plotted in black while anti-modes are in gray.

In the case of FOF the snake like contour mentioned above is seen to be modulated by the filter profile. This is due to the envelope f in (5) modulating the sine function [see Fig. 5(b)]. This means that, for a given ω_0, the number of external cavity modes is now strongly dependent on the detuning of ω_0 with respect to ω_m. For the frequency ω_0 far away from the central frequency ω_m of the filter, $f(\Delta\omega)$ will be almost zero, and there will only be a few solutions, while several modes are available for $\omega_0 \sim \omega_m$. Another difference is the phase shift introduced by $\arctan(\Lambda/(\Delta\omega - \omega_m))$. This term does not exist in the COF case, and it is a consequence of the Kramers–Kronig relation applied to the Lorentzian filter.

VI. Simulations

To simulate the experiment, the filter frequency is fixed, and the solitary laser frequency, i.e., the current, is varied. Fixed-point analysis is a crucial first step if one is to understand the dynamical behavior of such a nonlinear system. However, fixed points must be investigated for their stability, which, due to the high dimensionality of the system, is virtually impossible to do analytically. Therefore, simulations are needed to obtain a complete picture of the dynamics. In the following, the solutions of (5) will be referred to as fixed points, whereas the set of values (E, F, n) obtained by direct integration of (2) (the so-called simulation) is called the operation point.

Simulations were performed using (2). A modified fourth-order Runge-Kutta method was used to integrate the system. The solutions of (5) were used as the initial conditions. The external-cavity round-trip time was fixed so that the number of fixed point solutions were dependent only on the feedback level and the filter detuning. In agreement with experiment, the pump current was varied a few percent around 1.6 $J_{\rm thr}$. The external-cavity round-trip time was $\tau = 12.53$ ns corresponding to a 80-MHz FSR. The FWHM of the filter 2Λ is fixed to 0.64 GHz and the central frequency of the filter is fixed to $\omega_m = 540$ GHz above the solitary laser threshold frequency $\omega_{\rm thr}$ throughout these simulations. The values of all the parameters used are summarized in Table I.

TABLE I
Parameter Values Used in the Simulation

Parameter	Value
Linewidth enhancement factor (α)	5
Carrier lifetime (T_1)	167.88 ps
Differential gain (ξ)	$2.142 \cdot 10^{-8}$ ps^{-1}
Threshold current (J_{thr}/e)	$1.402 \cdot 10^{5}$ ps^{-1}
Photon decay rate (Γ_0)	0.357 ps^{-1}
Filter FWHM (2Λ)	640 MHz
Round trip time (τ)	12.53 ns

The dynamics were investigated for almost zero, low, moderate, and high feedback levels. For each case, two figures will be presented. One figure shows the frequency $\omega = \omega_0 + \Delta\omega$ of the DL with feedback versus the solitary laser frequency ω_0 which is directly proportional to the pump current J [see (3)]. The other figure shows the power transmitted through the filter versus time while the pump current is modulated with a ramp. Thus, we are able to compare directly this simulation with the experimental results.

1) *Almost zero feedback:* In this case, C is smaller than or about equal to 1; there is only one fixed point. As can be seen from Fig. 6(a), the frequency of the FOF system is hardly different from ω_0.
2) *Low feedback:* In Fig. 6(b), the system frequency ω versus ω_0 is shown for $C = 5$. Increasing ω_0 from ω_A moves the operation point from A to B where it jumps to C (see the upper left inset of Fig. 6(b)). Further increasing ω_0 moves the operation point from C to D where it jumps again to E. This type of behavior is repeated with the next external-cavity modes (e.g., E to F and then to G). Section A-B is part of an external-cavity mode and a jump, indicated by a filled arrow, is a switch from one external-cavity mode to the next one. The directions of the open arrows indicate the direction of time.

   For decreasing ω_0 a similar process happens: the operation point goes from G to H and finally to K through section I-J of an external-cavity mode with mode jumps between H and I, and between J and K. This phenomenon is observed for ω_0 in the vicinity of ω_m but disappears far away from it [see the lower right inset of Fig. 6(b)]. The mode jumps occur when a pair of fixed points is annihilated in a saddle-node bifurcation. After the annihilation, the system jumps to the closest available stable fixed point.
3) *Moderate feedback:* Fig. 6(c) shows the result of a simulation for $C = 80$. The external-cavity mode structure is shown as the solid line while the operation points obtained from the simulation are given by circles. Increasing ω_0 from ω_A gives rise to the same behavior described for the low feedback case: The system locks on one external-cavity mode A-B and then jumps to the next mode in C where it again locks on C-D. However, when ω_0 reaches ω_H, a big frequency jump equivalent to several external-cavity mode spacings occurs. This is a consequence of the negative slope of the envelope indicated with the dashed curve. As soon as the slope becomes positive, the external-cavity mode-locking process occurs again, as can be seen between I and J.

   There is a certain switching time involved in the process of jumping from one external-cavity mode to another. According to (2), several time scales can be identified in the dynamics. The exchange of energy between the field and the inversion is governed by the relaxation-oscillation frequency ($\omega_{RO} = 3.2$ GHz) and its damping rate (typically corresponding

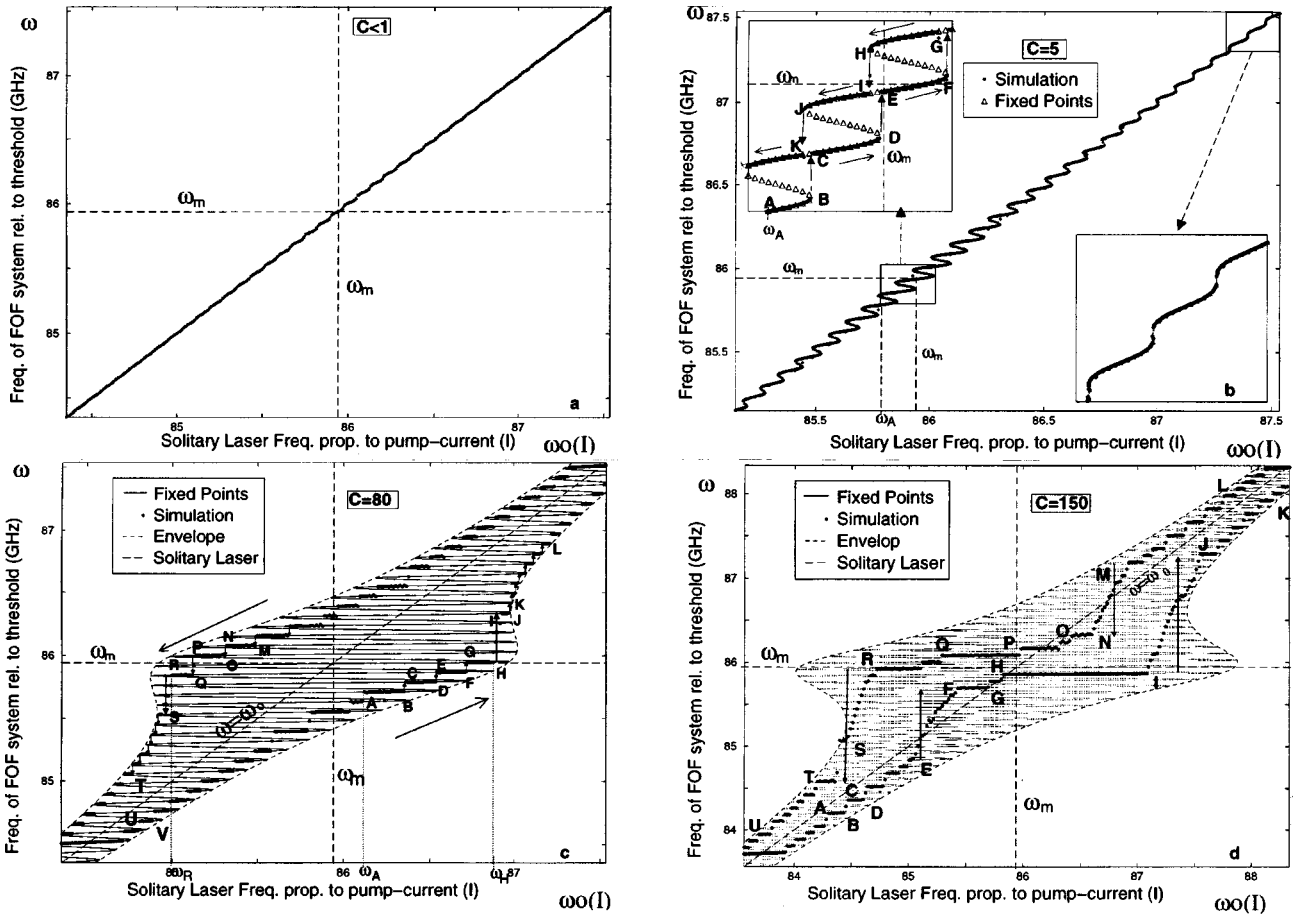

Fig. 6. The frequency ω of the DL plotted versus the solitary laser frequency ω_0 in the case of FOF for different levels of feedback. (a) $C < 1$ (–50 dB). (b) $C = 5$ (–42 dB). (c) $C = 80$ (–30 dB). (d) $C = 150$ (–27 dB). Here ω_m is the central frequency of the filter. Circles are the operational points of the DL obtained by simulation. Open arrows indicate the scanning direction. Filled arrows are the frequency jumps.

to 1 GHz–10 GHz). The external-cavity round-trip time τ and the feedback rate γ are two other time constants, the latter typically in the range 10 MHz–10 GHz. In addition, there is a time constant connected to the filter width which is equal to 0.64 GHz. The fastest time constant is given by the internal round-trip time of the DL and is typically $\tau_{in} \sim 5$ ps which is included in γ [14]. The switching time will in general depend on these time constants. Since all the corresponding relaxation mechanisms participate in the switching process, an investigation of the switching time requires a complete stability analysis. However, the time scale on which the switching occurs will be limited by the internal round-trip time $\tau_{\rm in}$ and the external round-trip time τ.

For decreasing ω_0, the system also locks to external-cavity modes. This is indicated on sections M-N, O-P, and Q-R. Mode jumps similar to what has been described above is observed at N and P. When $\omega_0 \simeq \omega_R$, a big frequency jump over several external-cavity mode spacings occurs. Note that the frequency ω_R is different from ω_H. Further, the path followed for decreasing ω_0 is different compared to the case with an increasing ω_0. This is a clear demonstration of hysteresis in the frequency domain induced by the filter. Note that the operation points are located close to, but not exactly on, the envelope, and that the lengths of the solitary laser frequency range (i.e., A-B) close to the positive flank of the filter are larger than those far away (U-V). This can be seen as a locking on the filter flank.

4) Strong feedback: The result of the simulation in the case of $C = 150$ is shown in Fig. 6(d). Here, the operation points are located around the external-cavity modes closest to ω_m. Furthermore, the operation points are located far away from the envelope of the filter. Note also that, in contrast to the situation of moderate feedback, the frequency of the DL experiences a jump on both flanks of the resonance peak of the filter, i.e., E-F and I-G for increasing ω_0 and M-N and R-S for decreasing ω_0.

Fig. 7 shows the power in the external cavity after filtering. This corresponds to the signal measured with PD1 in the experiment (see Fig. 1). Similar to the experiment, the current is scanned up and down with a ramp shown as dashed lines in the upper part of every figure. The scanning range has been chosen so as to scan a frequency range that includes the filter resonance. The four cases shown in Fig. 7(a)–(d) are the same as those in Fig. 6.

In Fig. 7(a), the $C \leq 1$ situation is depicted. The simulation shows that the DL traces out the filter profile.

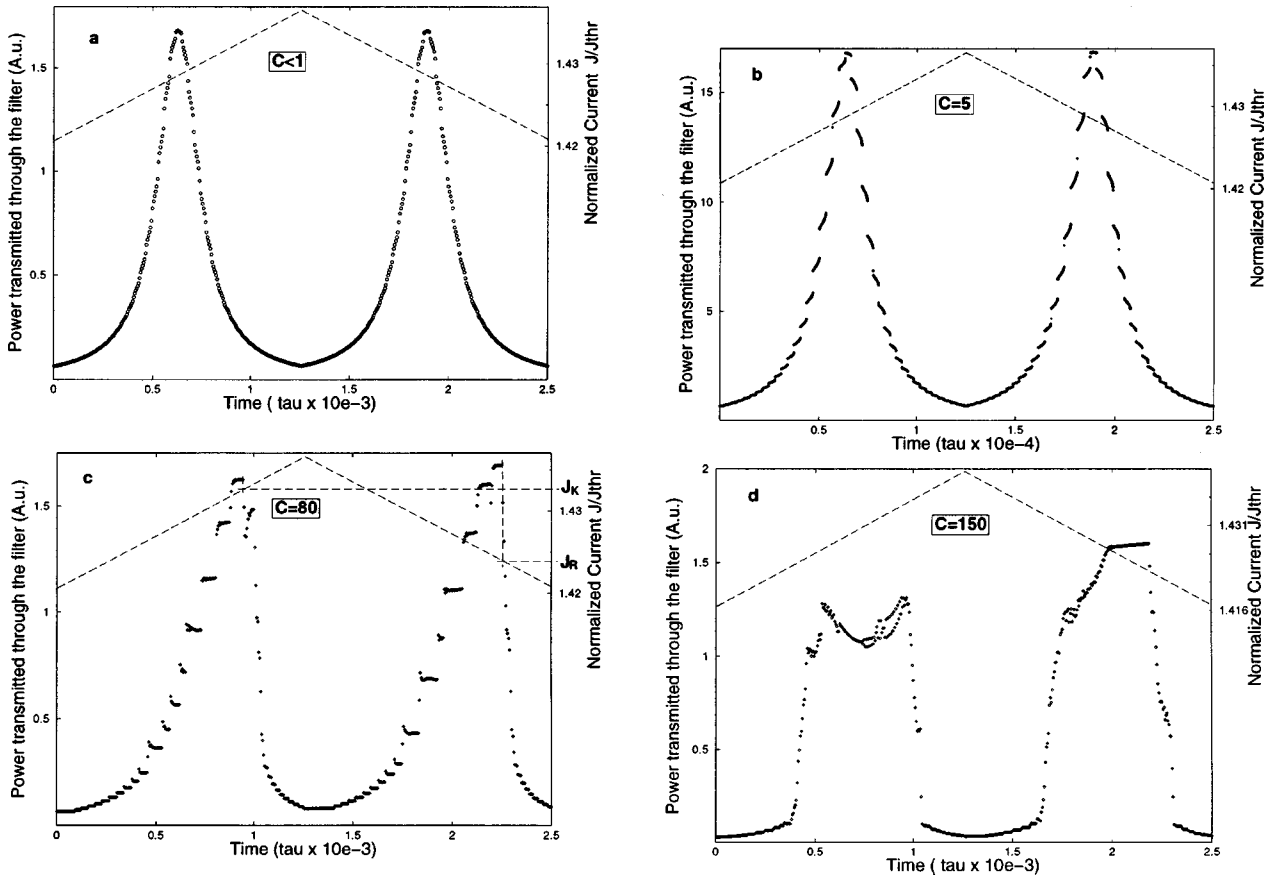

Fig. 7. Simulation of the power in the external cavity (open circles) versus time when the pump current (dashed line) is scanned up and down. (a) $C < 1$ (–50 dB); (b) $C = 5$ (–42 dB); (c) $C = 80$ (–30 dB) and (d) $C = 150$ (–27 dB).

The case with $C = 5$ is plotted in Fig. 7(b). In contrast to what is observed in Fig. 7(a), the power shows discrete operation levels. These segments correspond to the external-cavity modes similar to the segments A-B, C-D, etc., as described above [see Fig. 6(b)]. Note that seven modes are visible inside the FWHM, as expected from the ratio between the 0.64-GHz FWHM of the filter and the 80-MHz external-cavity mode spacing.

The case with $C = 80$ is shown in Fig. 7(c). The same external-cavity structure as in the case of low feedback is observed. However, two asymmetries are now visible. First, a jump is observed on the right side of the filter profile whereas the left side exhibits the external-cavity mode structure. These jumps are direct consequences of the H-I and R-S frequency jumps shown in Fig. 6(c). Second, the jumps occur for different values of the current indicated by J_R and J_H in Fig. 7(c) corresponding, respectively, to ω_R and ω_H in Fig. 6(c). The difference between J_R and J_H is an evidence of hysteresis.

The strong feedback case $C = 150$ is shown in Fig. 7(d). The external-cavity mode structure has now disappeared completely and the system frequency jumps directly from the foot of the filter profile to the top $(\omega \sim \omega_m)$, where it locks until it jumps back again. Two asymmetries can be observed. The left peak, i.e., for increasing current, has a lower amplitude than the right peak. In addition, there are signs of instabilities at the top of the left peak that are absent for the right peak. Note that the operation points now cross the $\omega = \omega_0$ line. This is in contrast to the previous situations where the operation points were on the right (left) side of the line when scanning the current up (down). Thus, the strong feedback introduces both red and blue shifts with respect to the solitary laser frequency for increasing and decreasing currents.

TABLE II
DOMAINS INVESTIGATED EXPERIMENTALLY AND THEORETICALLY

Domain	C	Experiment	Theory
No feedback	< 1	-55 dB	-50 dB
Low feedback	5	-40 dB	-42 dB
Moderate feedback	80	-31 dB	-30 dB
High feedback	150	-29 dB	-27 dB

VII. DISCUSSION

The different regions studied experimentally and theoretically are summarized in Table II. Without any feedback or for very small amounts of feedback $(C < 1)$, the experimental and theoretical figures show very similar filter profiles [see Figs. 2(a) and 7(a)]. In the experiment, a FP-type filter, characterized by several resonances separated by the FSR, was used. Since these resonances are separated in frequency by distances that are large compared to the linewidth of the DL, there is

no interaction between the resonances and they can hence be considered individually.

For low feedback ($C = 5$, –40 dB for the experiment), the simulation and the experiment both show the external-cavity mode structure, see Figs. 2(b) and 7(b). The number of external-cavity modes within the filterwidth is in both experiment and simulation determined by the ratio of the filterwidth and the external-cavity mode spacing.

In the moderate feedback case ($C = 80$, –31 dB for the experiment), shown in Fig. 2(c) for the experiment and in Fig. 7(c) for the simulation, the frequency jump over several external-cavity modes is observed in both. The feedback levels are on the same order of magnitude and good agreement between simulation and experiment is obtained. However, the difference in peak height for increasing and decreasing currents is more pronounced in the experiment than in the simulation. A difference in the α-parameter value may explain this difference.

For higher feedback levels ($C = 150$, –29 dB for the experiment), the simulation starts to differ more from the experimental data. From the experiment, the DL can be seen to lock to only one of the external-cavity modes, see Fig. 2(d). This point is confirmed by the simulation [see Figs. 7(d) and 6(d)]: the DL makes a frequency jump from the foot of the filter and locks onto an external-cavity mode. The operation point of the DL can be seen to lie on two external-cavity modes. Following locking, the DL frequency jumps over several external-cavity modes and relaxes to the almost free-running case. It can be noted that the experimentally observed difference between peak amplitudes when scanning the current up and down is now strongly pronounced. This is not the case in the simulation. Note further that the experiment indicates the beginning of the undamping of the relaxation oscillation. The differences may be due to the presence of noise, which was not accounted for in the simulation.

For very high feedback (–26 dB), the experiment shows a strong undamping of the relaxation oscillation [see Fig. 2(e)]. Furthermore, longitudinal mode jumps were also observed. In this case, the model is not applicable since it assumes a single-mode operating laser.

Our model is also valid for filters narrower than the external-cavity mode spacing. Since there are not multiple cavity modes within the filter, jumps between these cannot be observed. According to (5), we expect the laser to lock to the filter even if it is not coinciding with an external-cavity mode. The time scale induced by the filter width will, in this case, limit the dynamics of the system giving rise to an increased stability similar to what has been observed by [9]. For very narrow filters, it is expected that the feedback level can never reach the amount where the relaxation oscillation becomes undamped because of the saturation process mentioned in Section IV.

VIII. Conclusion

We have presented a combined experimental and theoretical study of delayed, filtered optical-feedback effects on diode lasers.

Experimentally, we have demonstrated that the frequency of a diode laser exposed to feedback filtered by a FP type of filter locks to the filter profile through the external-cavity modes selected by the filter. As the feedback rate is increased, this locking behavior is overtaken by frequency jumps corresponding to several external-cavity modes. This phenomenon was observed to lead to hysteresis and multistability. For higher amounts of feedback, the frequency spectrum of the diode laser was observed to show undamped relaxation oscillations at 3.2 GHz. This is the result of a Hopf bifurcation. This kind of dynamics has been summarized in a stability diagram. Narrowing the filter width was observed to suppress the undamping of the relaxation oscillation and thus may be a powerful way to control the dynamics.

To explain the experimental results, a theoretical model based on the new set of rate equations proposed in [12] and a pump-dependent diode laser frequency was adopted. The model reproduces the observed external-cavity mode locking, hysteresis, frequency jump, and multistability. The switching time of the frequency jump is speculated to be in the nanosecond range. This point will be investigated further. We believe that filtered optical feedback has potential applications in optical telecommunications and optical signal processing where frequency locking and hysteresis are of great importance. The prevention of relaxation-oscillation undamping due to filtering may serve as a possible means of controlling chaos.

References

[1] F. Mogensen, H. Olesen, and G. Jacobsen, "Locking conditions and stability properties for a semiconductor laser with external light injection," *IEEE J. Quantum Electron.*, vol. QE-21, pp. 784–793, 1985.

[2] R. Lang and K. Kobayashi, "External optical feedback effects on semiconductor injection laser properties," *IEEE J. Quantum Electron.*, vol. QE-16, pp. 347–355, 1980.

[3] K. Vahala, K. Kyuma, A. Yariv, S. Kwong, M. Cronin-Colomb, and K. Y. Lau, "Narrow linewidth single frequency semiconductor laser with phase conjugate external cavity mirror," *Appl. Phys. Lett.*, vol. 49, pp. 1563–1565, 1986.

[4] G. P. Agrawal and N. K. Dutta, *Long Wavelength Semiconductor Lasers*. New York: Van Nostrand Reinhold, 1986.

[5] L. Goldberg, H. F. Taylor, A/ Dandridge, J. F. Weller, and R. O. Miles, "Spectral characteristics of semiconductor lasers with optical feedback," *IEEE J. Quantum Electron.*, vol. QE-18, pp. 555–563, 1982.

[6] R. W. Tkach and A. R. Chraplyvy, "Regimes of feedback effects in 1.5 μm DFB lasers," *J. Lightwave Technol.*, vol. LT-4, pp. 1655–1661, 1986.

[7] J. Mørk, M. Semkow, and B. Tromborg, "External optical feedback effects on semiconductor injection laser properties," *Electron. Lett.*, vol. 26, pp. 609–610, 1990.

[8] M. Kozuma, M. Kourogi, and M. Ohtsu, "Frequency stabilization, linewidth reduction, and fine detuning of a semiconductor laser by using velocity-selective optical pumping of atomic resonance line," *Appl. Phys. Lett.*, vol. 61, pp. 1895–1897, 1992.

[9] R. Loe-Mie, A. V. Papoyan, A. M. Akulshin, A. Lezama, J. R. Rios Leite, O. Lopez, D. Bloch, and M. Ducloy, "Nearly all-optical frequency-stabilization of a laser diode on the 120 kHz intercombination line of Ba," *Opt. Commun.*, vol. 139, pp. 55–59, 1997.

[10] B. Dahmani, L. Hollberg, and R. Drullinger, "Frequency stabilization of semiconductor lasers by resonant optical feedback," *Opt. Lett.*, vol. 12, pp. 876–878, 1987.

[11] O. K. Andersen, A. P. A. Fischer, I. C. Lane, E. M. Louvergneaux, S. Stolte, and D. Lenstra, "Experimental stability diagram of a diode laser subject to weak phase-conjugate feedback from a Rubidium vapor cellk," *IEEE J. Quantum Electron.*, vol. 35, pp. 577–582, 1999.

[12] M. Yousefi and D. Lenstra, "Dynamical behavior of a semiconductor laser wity filtered external optical feedback," *IEEE J. Quantum Electron.*, vol. 35, pp. 970–977, 1999.

[13] D. Lenstra, M. van Vaalen, and B. Jaskorzynska, "On the theory of a single-mode laser with weak optical feedback," *Physica C*, vol. 125, pp. 255–264, 1984.

[14] G. A. Acket, D. Lenstra, A. J. den Boef, and B. H. Verbeek, "The influence of feedback intensity on longitudinal mode propertis and optical noise in index-guided semiconductor lasers," *IEEE J. Quantum Electron.*, vol. QE-20, pp. 1163–1169, 1984.

Alexis P. A. Fischer was born 1969 in Lyon, France. He received the M.Sc. degree in engineering in 1993, the D.E.A. degree in 1994 from the University of Franche-Comte, Besancon, France, and the Ph.D. degree from the Optics Laboratory P. M. Duffieux, Besancon, France, in 1998. His doctoral research focused on electronical and optical feedback in semiconductor lasers for telecommunication applications.

He is currently working on semiconductor lasers with feedback in the group of D. Lenstra, Faculty of Sciences, Vrije Universiteit Amsterdam, The Netherlands. His interests are optical telecommunications, signal routing, tunable semiconductor lasers, wavelength switching, laser frequency stabilization, electronical and optical feedback, phase conjugate feedback, laser dynamics, and chaos.

Ole K. Andersen was born in 1970 in Aarhus, Denmark. He received the M.Sc. degree from the Oersted Laboratory, University of Copenhagen, Denmark, in 1995. He is currently working toward the Ph.D. degree on phase-conjugate feedback effects on diode laser dynamics in the groups of Prof. D. Lenstra and Prof. S. Stolte at the Vrije Universiteit, Amsterdam, The Netherlands.

His research interests are diode lasers with conventional feedback and the studies and applications of chaos.

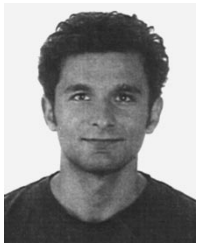

Mirvais Yousefi was born on July 5, 1975, in Kabul, Afghanistan. He recieved the M.Sc. degree in theoretical physics from the University of Lund, Sweden, in 1998. He is currently working toward the Ph.D. degree in the theory group at the Department of Quantum Optics, Vrije Universiteit, Amsterdam, The Netherlands.

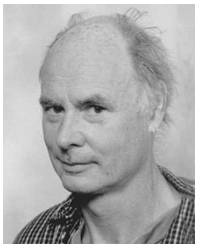

Steven Stolte was born in 1943 in Utrecht, The Netherlands. He received the M.Sc. and Ph.D. degrees from The Catholic University of Nijmegen in 1967 and 1972, respectively.

His post-doctoral study on reaction-dynamics of long-lived complexes was carried out in the group of Prof. R. B. Bernstein (1972–1974) at the University of Wisconsin, Madison, and at the University of Texas, Austin. As a Senior Scientist, he returned to the molecular and laser physics group in Nijmegen where he broadened his research expertise in a study of the laser frequency and power dependence for the infrared multiphoton excitation of small molecules and clusters and CW-overtone Raman spectroscopy of high-lying states. In 1989, he was appointed to Full Professor in Experimental Laser Spectroscopy in the Department of Physical and Theoretical Chemistry at the Vrije Universiteit, Amsterdam, The Netherlands. There, in 1990, he started a new group aimed at laser spectroscopy studies of matter.

Prof. Stolte is a member of the Dutch and German Physical Societies. He served as chairman of The Molecular Physics Section of the atomic and molecular physics section of the European Physical Society (1990–1992).

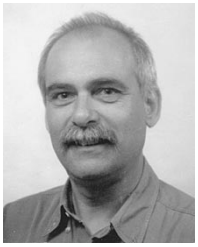

Daan Lenstra was born in Amsterdam, The Netherlands, in 1947. He received the M.Sc. degree in theoretical physics from the University of Groningen, The Netherlands, and the Ph.D. degree from Delft University of Technology, The Netherlands. His dissertation work was on polarization effects in gas lasers.

He was with Delft University of Technology during 1975–1984 and with Eindhoven University of Technology during 1984–1991. He was a Research Associate at the University of Rochester, Rochester, NY, from 1981 to 1982 and a Guest Scientist in 1984 at Philips Research Laboratories, Eindhoven, The Netherlands. From 1989 to 1991, he was appointed part-time Professor at the University of Leiden, The Netherlands, and, since 1991, he has held a chair in theoretical quantum electronics at the Vrije Universiteit, Amsterdam. Since 1979, he has researched topics in quantum electronics and solid-state physics, such as photon statistics in resonant fluorescence, coherent electron transport, resonant tunneling, semiconductor lasers, and analogies between optics and microelectronics. His present interests are fundamental nonlinear dynamics in semiconductor lasers and quantum optics in small semiconductor structures.